9th International Conference on Fracture Mechanics of Concrete and Concrete Structures
FraMCoS-9
V. Saouma, J. Bolander, and E. Landis (Eds)
DOI 10.21012/FC9.266

TRANSPORT-STRUCTURAL MODELLING OF CORROSION INDUCED CRACKING

CAROLINE FAHY*, DOMENICO GALLIPOLI†, SIMON J. WHEELER* AND PETER GRASSL*

*University of Glasgow
Glasgow, UK
e-mail: peter.grassl@glasgow.ac.uk

†Université de Pau et des Pays de l'Adour
Anglet, France
email:domenico.gallipoli@univ-pau.fr

Key words: Fracture, Corrosion, Concrete, Hydro-Mechanical

Abstract. Transport of corrosion products into pores and cracks in concrete must be considered when predicting corrosion induced cracking in reinforced concrete structures, since this transport significantly delays the onset of cracking and spalling by reducing the amount radial displacement displacement imposed on the concrete at the steel/concrete interface. We aim to model this process by means of a transport-structural approach, whereby the transport part is driven by a pressure gradient generated by the volumetric expansion due to the transformation of steel into corrosion products. This pressure driven transport was introduced in an analytical axisymmetric thickwalled cylinder model and a numerical network approach. The influence of cracking and permeability on corrosion induced cracking process with increasing inner displacement is investigated with these two approaches.

1 INTRODUCTION

Corrosion induced cracking is the most commonly encountered deterioration mechanism in reinforced concrete structures, which involves the transformation of steel reinforcement into corrosion products, which occupy a greater volume than the original steel. This volume expansion due to this chemico-mechanical process results in internal pressure acting on the concrete, which is equilibrated by circumferential tensile stresses leading to cracks in, and potentially spalling of the concrete. Understanding corrosion induced cracking in concrete is difficult because of multiple interacting processes and phenomena, such as the transport of corrosion products into pores and cracks, the spatial distribution of steel areas affected by corrosion, compaction of corrosion products, the influence of the chemical environment on the rust products, and creep, shrinkage and cracking of concrete.

The transport of corrosion products into pores and cracks in concrete must be considered when predicting corrosion induced cracking in reinforced concrete structures, since this transport significantly delays the onset of cracking and spalling by reducing the amount radial displacement displacement imposed on the concrete at the steel/concrete interface. The entire process of corrosion induced cracking is commonly divided into initiation and propagation phases [21], whereby the propagation is characterised by the progression from corrosion initiation, surface cracking, spalling and eventually structural collapse either due to loss of

anchorage or reinforcement rupture (Figure 1). The present work is focused on the propagation phase by modelling the transport of corrosion products into the concrete and its influence on the process of corrosion induced cracking.

Physical tests on corrosion induced cracking have been reported for single and multiple reinforcement bars in [2, 1, 15]. Experimental studies on the transport of corrosion products have been performed in [24] and [13]. The modelling approaches can be categorised into analytical models mainly focusing on obtaining compact solutions for specimens with simple geometries [3, 11, 17] and numerical models applicable to general geometries and boundary conditions [14, 12, 20, 16, 18].

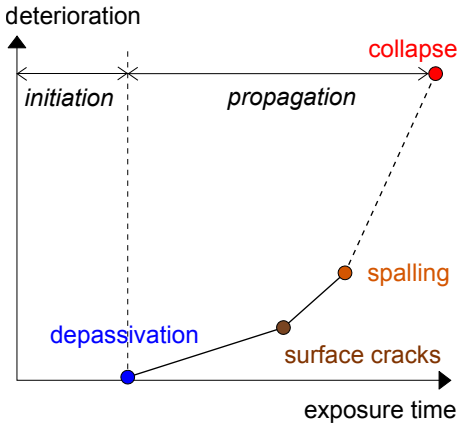

Figure 1: Corrosion induced cracking: Service life definition after Tuutti [21].

In both analytical and numerical models, the transport of corrosion products into the concrete has been considered in different ways. In many approaches, a porous zone was considered which had to be filled before the volume expansion due to the transformation from steel into corrosion products started to generate pressure in the surrounding concrete [11, 8]. Other studies proposed to fill voids and cracks once corrosion induced cracking had started [6, 20]. However, these modelling approaches do not describe the rust transport by a mechanistic approach, but instead use adhoc rules to describe the penetration of the rust. One exception to this is the work reported in [16] in which diffusion is used to describe the transport of rust into the concrete.

The aim of the present work is to model the mechanics of the transport of rust into concrete by a transport-structural approach, whereby the corrosion products are transported into the concrete by means of a pressure gradient originating from the volume expansion due to the transformation from steel into corrosion products. To the authors' knowledge, this approach has not been proposed before.

The transport-structural modelling of corrosion induced cracking is introduced here both in an analytical axisymmetric thick-walled cylinder approach for describing the stage from initiation to surface cracking and a discrete network approach, which, in principle, is capable of describing the full propagation phase (Figure 1). The analytical thick-walled cylinder model is an extension of previous analytical models reported in [17]. The network model belongs to the group of discrete element approaches, for which the connectivity between elements remains the same during the analysis [19, 5, 7]. They also often called lattice or rigid body spring networks. Network models have been shown to be capable of describing fracture and transport in concrete mesh-independently and capable of modelling the coupling of fracture and transport [4, 9, 10].

2 CORROSION PRODUCTS AT STEEL/CONCRETE INTERFACE

The key novelty of the present work is that the pressure driven flow of corrosion products into the concrete is considered when modelling the formation of corrosion products at the steel/concrete interface. For this new approach, the main assumptions are that the corrosion products are an incompressible fluid with a time independent viscosity. Concrete is assumed to be fully saturated and Biot's coefficient for the porous concrete is assumed to be zero.

The overall approach for the modelling of the volume expansion associated with the transformation from steel into corrosion products is

to apply an increment of Eigen-displacement Δu_{cor} at the interface between the steel and concrete, which results in a reactive pressure P_{fi} in the mechanical part of the model. This pressure is then used to determine the flow of corrosion products into the concrete by the transport part of the model. With this approach, the mechanical analysis is independent of the transport part. In Figure 2, the decomposition into different components is illustrated. For a time increment Δt, the volume balance is

$$\alpha \Delta x_{\mathrm{cor}} = \Delta x_{\mathrm{cor}} + \Delta u_{\mathrm{cor}} + q \Delta t \qquad (1)$$

Here, the total increment of volume of corrosion products is $\alpha \Delta x_{\mathrm{cor}}$, where Δx_{cor} is the increment of radius that is removed from the steel bar and α is an expansion factor, describing the volume increase due to the transformation from steel into corrosion products. The mechanical part is $\Delta u + \Delta x_{\mathrm{cor}}$, where Δu is the increment of prescribed radial Eigen-displacement. The remaining part is transported into the pores and cracks of the concrete, which is $q\Delta t$. Here, $q = Q/(2\pi r_{\mathrm{i}} t)$ is the flux of corrosion products at the steel/concrete interface, whereby Q is the total flow and r_i is the radius of the reinforcement bar.

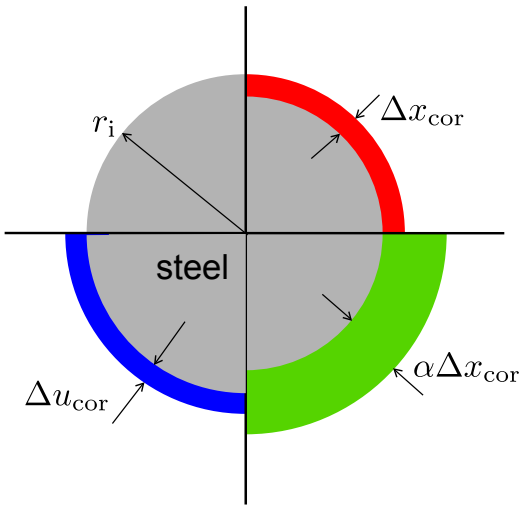

Figure 2: Corrosion products at steel/concrete interface: Steel reinforcement bar with layers illustrating the split into different corrosion product components.

Assuming that the entire applied corrosion current density i_{cor} is consumed in the corrosion process, the increment of loss of radius Δx_{cor} can be related to the corrosion rate through Faraday's law where

$$\Delta x_{\mathrm{cor}} = 0.0315 i_{\mathrm{cor}} \Delta t \qquad (2)$$

in which 0.0315 is a factor converting the units of i_{cor} from μA/cm^2 into μm/days as used in [14]. Substituting Δt form (2) in (1) and solving for Δx_{cor} gives

$$\Delta x_{\mathrm{cor}} = \frac{\Delta u_{\mathrm{cor}}}{\alpha - 1 - q/(0.0315 i_{\mathrm{cor}})} \qquad (3)$$

In the following section, this approach is used within the analytical and network model, respectively.

3 ANALYTICAL MODEL

The analytical model is based on an axisymmetric formulation of a thick-walled cylinder using orthotropic elasticity following the work in [22, 17]. The main approach is to divide the thick-walled cylinder into an inner cracked and outer uncracked region (Figure 3). For the cracked region, orthotropic elasticity is used [17], whereas the uncracked region is modelled with isotropic elasticity [22]. The orthotropy for the cracked cylinder is introduced by reducing the tangential Young's modulus by means of a scalar damage model, which is driven by an exponential stress-crack opening law.

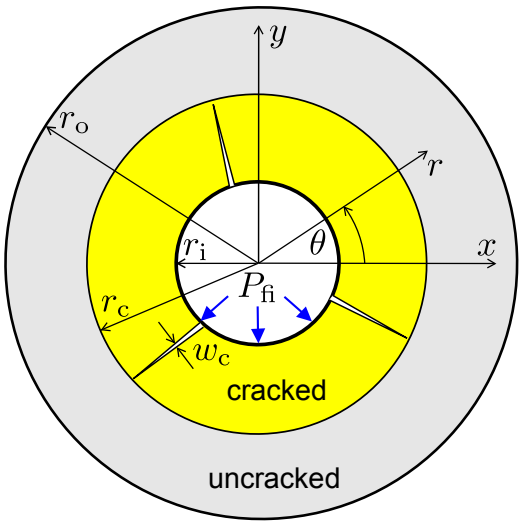

Figure 3: Analytical model: Axisymmetric thick-walled cylinder divided into an inner cracked and outer uncracked part.

The main equation for the mechanical part of the thick-walled cylinder model for both cracked and uncracked region is the second order ordinary differential equation

$$\frac{d^2u}{dr^2} + \frac{1}{r}\frac{du}{dr} - \frac{E_\theta}{E_\mathrm{r}}\frac{u}{r^2} = 0 \tag{4}$$

whereby u is the radial displacement, r is the radial coordinate and $\frac{E_\theta}{E_\mathrm{r}}$ is the ratio of circumferential and radial Young's moduli. This ratio is related to the damage parameter ω as

$$\frac{E_\theta}{E_\mathrm{r}} = 1 - \omega \tag{5}$$

For the uncracked region, $\omega = 0$ so that (4) is linear. For the cracked region, ω is a nonlinear function of the radius and the radial displacement, which is controlled by an inelastic strain

$$\varepsilon_\mathrm{f} = n_\mathrm{c}\frac{w_\mathrm{f}}{l_\mathrm{c}} = n_\mathrm{c}\frac{w_\mathrm{f}}{2\pi r} \tag{6}$$

Here, w_f is the crack opening threshold in the exponential stress crack opening law which is related to the fracture energy G_F and the tensile strength f_t as $w_\mathrm{f} = G_\mathrm{F}/f_\mathrm{t}$, and n_c is the number of cracks assumed to be present in the thick-walled cylinder.

For each part of the cylinder, two boundary conditions are required to solve the second order differential equation. For the outer uncracked cylinder, the conditions are that the radial stress at the boundary is equal to zero ($\sigma_\mathrm{r}(r = r_\mathrm{o}) = 0$) and the tangential stress at the boundary between cracked and uncracked region is equal to the tensile strength ($\sigma_\theta(r = r_\mathrm{c}) = f_\mathrm{t}$). The two conditions for the cracked cylinder are that the two radial stresses at the boundary between cracked and uncracked region are equal ($\sigma_\mathrm{r}(r = r_\mathrm{c}^+) = \sigma_\mathrm{r}(r = r_\mathrm{c}^-)$) and the tangential stress at the boundary between cracked and uncracked region is equal to the tensile strength ($\sigma_\theta(r = r_\mathrm{c}) = f_\mathrm{t}$). For the uncracked part, (4) can be solved explicitly. However, for the cracked part, a finite difference scheme is used to obtain the solution numerically. The two solutions of the radial displacement u of the two regions are obtained for an incrementally increasing radius r_c. From u, the radial and tangential stresses and strains are obtained [22]. Furthermore, the crack openings as a function of r can be determined as

$$w_\mathrm{c} = \frac{l_\mathrm{c}}{n_\mathrm{c}}\omega\varepsilon_\theta = \frac{2\pi r}{n_\mathrm{c}}\omega\frac{u}{r} \tag{7}$$

This crack opening is then used for the transport part of the model extending the analytical approach described in [10] to case of the cracked cylinder. The radial stress at the inner boundary ($\sigma_\mathrm{r}(r = r_\mathrm{i})$) is set equal to the fluid pressure P_fi, the spatial gradient of which in the radial direction is related to the total flow rate Q through the cylinder as

$$dP_\mathrm{f} = \frac{\mu}{\kappa}\frac{Q}{2\pi r t}dr \tag{8}$$

where μ is the dynamic viscosity of the corrosion products, which is the fluid transported through the thick-walled cylinder. Furthermore, κ is the permeability which is composed of a cracked and uncracked contribution as $\kappa = \kappa_0 + \kappa_\mathrm{c}(r)$, whereby

$$\kappa_\mathrm{c} = n_\mathrm{c}\xi\frac{w_\mathrm{c}^3}{12 l_\mathrm{c}} \tag{9}$$

is the cubic law [23] reduced by a factor ξ taking into account the influence of fracture roughness on the crack permeability.

4 NETWORK MODEL

The network model used in this study is very similar to the approach presented in [9, 10], and is here only briefly reviewed. The structural part consists of an irregular network of beam-like elements which are arranged based on the Delaunay tessellation of a random set of points (Figure 4a). Each element connects two nodes which each possess three degrees of freedom, namely two translations and one rotation. They are related to a discontinuity at the mid-point C of the mid-cross-section (Figure 4b). This displacement discontinuity is used to model the constitutive response of the elements. Identical to the analytical model in the previous section, the stress-crack opening law is chosen to be exponential with a crack-opening threshold w_f.

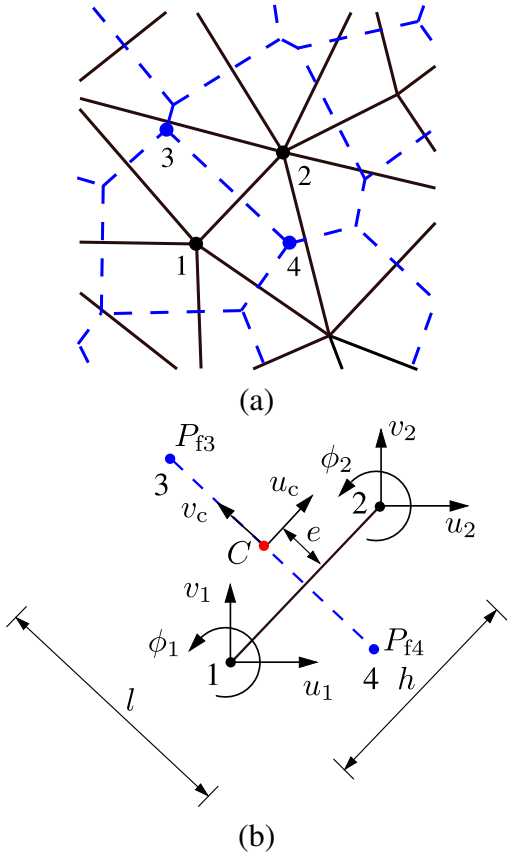

Figure 4: Network model: (a) Discretisation based on dual Delaunay and Voronoi tessellation, (b) Structural and transport elements.

For the transport part conduit elements are arranged in a network based on the Voronoi tessellation of the domain, which is dual to the network of structural elements. The constitutive response of the transport elements takes into account the transport through the uncracked and cracked material by means of the permeability $\kappa = \kappa_0 + \kappa_c$, as used in the analytical thick-walled cylinder model. A detailed description of how the boundary conditions between structural and transport lattices are enforced at the inner boundary can be found in [10].

5 ANALYSIS AND RESULTS

The two modelling approaches outlined above are applied to the failure process of a thick-walled cylinder subjected to an increasing inner radial displacement representing a layer of corrosion products. The aim of this analysis is to investigate the nonlinear relationship between the radial pressure and loss of diameter x_{cor}. The analyses are performed incrementally, whereby for each increment a sequence of structural and transport analyses are performed. Then, x_{cor} is determined by considering the applied radial displacement and transport contributions according to (3).

For all analyses, the same input parameters were chosen for the analytical and network model. The geometry of the thick-walled cylinder is chosen as $r_{\text{i}} = 8$ mm and $r_{\text{o}} = 58$ mm. The material parameters for the mechanical part are Young's modulus $E = 30$ GPa, Poisson's ratio $\nu = 0$, tensile strength $f_{\text{t}} = 3$ MPa and fracture energy $G_{\text{F}} = 0.15$ N/mm. For the structural part of the analytical model, it was also required to assume the number of cracks, which was chosen as $n_c = 4$ based on the results obtained from the network model. For the transport part, two permeabilities of the uncracked material were used to investigate the influence of this parameter on the loss of radius x_{cor}. The permeabilities were chosen as $\kappa_0 = 1 \times 10^{-10}$ and 5×10^{-10} mm^2. Furthermore, the other parameters for the transport part were selected as $\xi = 0.001$ and $\mu = 0.019$ MPas. Finally, the expansion factor of the corrosion products was assumed to be $\alpha = 2$ and $i_{\text{cor}} = 100$ μA/cm^2.

In Figure 5, the internal pressure P_{fi} versus the loss of radius x_{cor} for the two uncracked permeabilities κ_0 are shown for the two modelling approaches. The agreement between the two approaches is very good. The analytical model only slightly overestimates the maximum pressure obtained by the network model. Furthermore, k_0 has a strong influence on the P_{fi}-x_{cor} curve. For the greater permeability, the maximum pressure is reached at a greater x_{cor}. Although cracking strongly influences the P_{fi}-x_{cor} curve resulting in the nonlinear mechanical response, it was found to have a small influence of the overall permeability of the transport part for the present small crack openings ($w_{\text{c}}^{\max} < 0.1$ mm).

In Figure 5, three stages are marked at which the cracking is shown in Figure 6. The red and grey lines refer to active and inactive cracks, respectively. Here, an active crack is defined as a

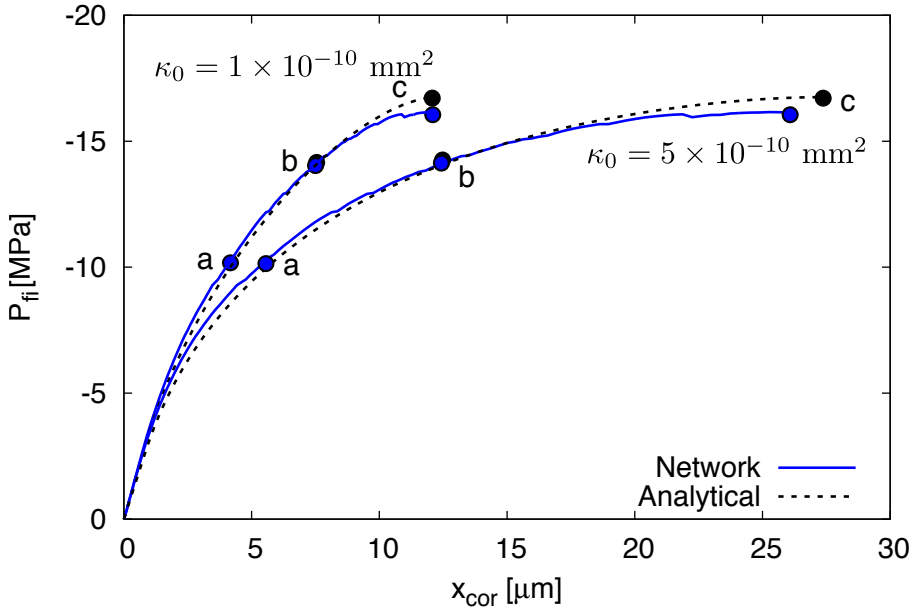

Figure 5: Internal pressure P_{fi} versus loss of radius x_{cor} for the network and analytical model. The three marked stages refer to crack patterns shown in Figure 6.

mid-crosssection at which damage increases at this stage of analysis. The dashed line shows the interface between the crack and uncracked region in the analytical model. It can be seen that there is again a very good agreement between the analytical and network model. For stage (c), the four main cracks from the network model do not have the same length anymore. This indicates the limit of the analytical model. Any further radial displacement at the inner boundary, would lead to a completely asymmetric crack pattern with only one crack remaining active. The crack patterns in Figure 5 apply to both analyses ($\kappa_0 = 1 \times 10^{-10}$ and 5×10^{-10} mm^2), since the structural part of the analysis is independent of transport part.

The strong dependence of x_{cor} on the permeability κ_0 is further illustrated by showing the ratio of increments of transported and total volumes of corrosion products versus the loss of radius for the two models in Figure 7. Again, a good agreement between the models is obtained. The greater the permeability, the greater is the volume of corrosion products transported into the concrete. At stage (c), the volume ratio predicted from the analytical model is greater than that from the network approach, since also the inner pressure of the analytical model is greater than from the network one.

6 CONLCUSIONS

A new transport-structural modelling approach to corrosion induced cracking has been proposed, which includes the pressure driven transport of corrosion products. This approach has been applied to both an analytical thick-walled cylinder model and a network model. The results of the two models are in very good agreement in the form of pressure versus radius loss, crack fronts and transported volumes versus radius loss. Whereas the analytical model is limited to axisymmetric situation, which appear to be valid up to the peak of the pressure-radius loss curves, the network model has the potential to predict the entire propagation phase up to spalling.

REFERENCES

[1] C Alonso, C Andrade, J Rodriguez, and José Miguel Diez. Factors controlling cracking of concrete affected by reinforcement corrosion. *Materials and structures*, 31(7):435–441, 1998.

[2] C. Andrade, C. Alonso, and F.J. Molina. Cover cracking as a function of bar corro-

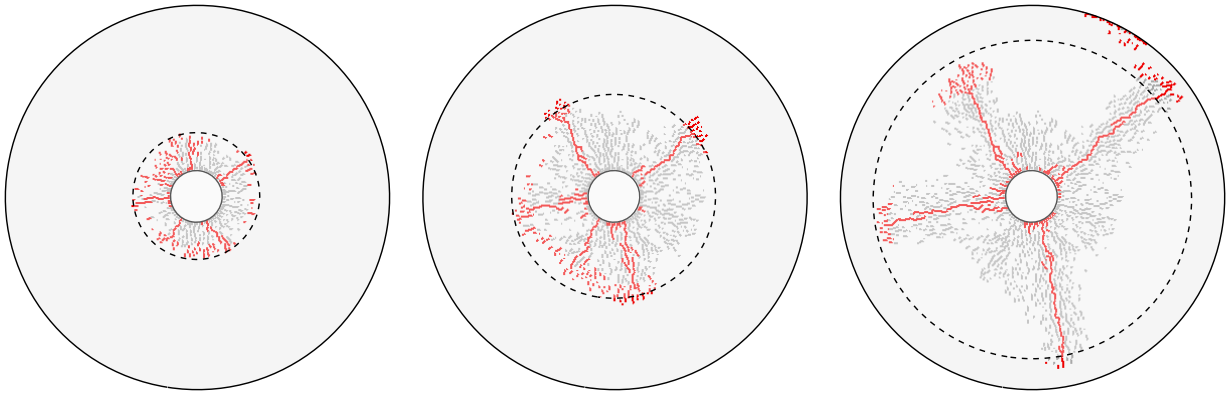

(a) (b) (c)

Figure 6: Crack patterns for three stages in the P_{fi}-x_{cor} curve shown in Figure 5. The red and grey lines show active and inactive cracks. The dashed line represents the interface between cracked and uncracked region of the analytical model.

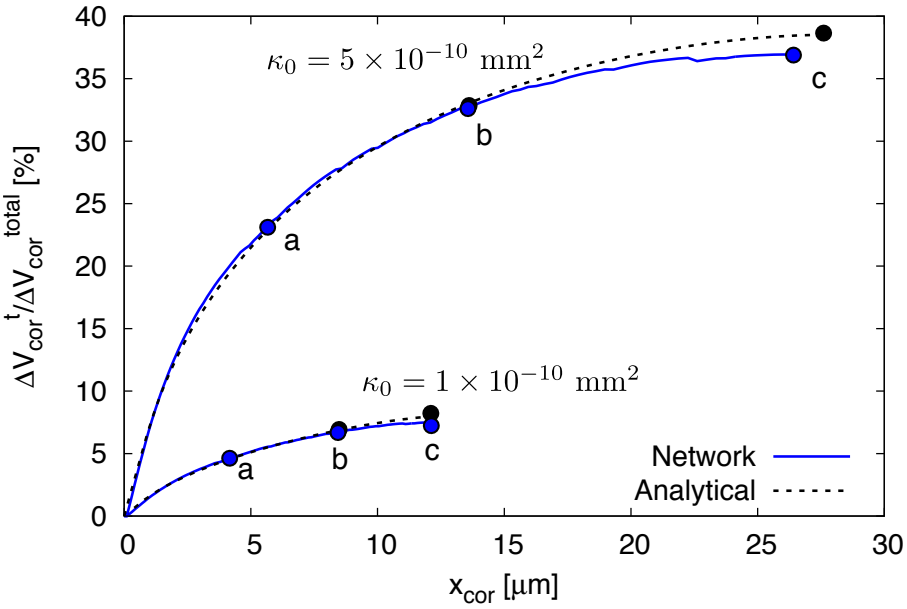

Figure 7: Ratio of increments of volume of transported and total volume of corrosion products versus radius loss x_{co} for the network and analytical model. The three marked stages refer to crack patterns shown in Figure 6.

sion: Part I-Experimental test. *Materials and Structures*, 26(8):453–464, 1993.

[3] Z. P. Bažant. Physical model for steel corrosion in concrete sea structures: application. *Journal of the Structural Division, ASCE*, 105(6):1154–1166, 1979.

[4] J. E. Bolander and S. Berton. Simulation of shrinkage induced cracking in cement composite overlays. *Cement and Concrete Composites*, 26:861–871, 2004.

[5] J. E. Bolander and S. Saito. Fracture analysis using spring networks with random geometry. *Engineering Fracture Mechanics*, 61:569–591, 1998.

[6] L. Chernin, D. V. Val, and K. Y. Volokh. Analytical modelling of concrete cover cracking caused by corrosion of reinforcement. *Materials and Structures*, 43(4):543–556, 2010.

[7] B. Damjanac, C. Detournay, and P. A. Cundall. Application of particle and lattice codes to simulation of hydraulic fracturing. *Computational Particle Mechanics*, pages 1–13, 2015.

[8] T. El Maaddawy and K. Soudki. A model for prediction of time from corrosion initiation to corrosion cracking. *Cement and Concrete Composites*, 29(3):168–175, 2007.

[9] P. Grassl. A lattice approach to model flow in cracked concrete. *Cement and Concrete Composites*, 31(7):454–460, 2009.

[10] P. Grassl, C. Fahy, D. Gallipoli, and S. J. Wheeler. On a 2d hydro-mechanical lattice approach for modelling hydraulic fracture. *Journal of the Mechanics and Physics of Solids*, 75:104–118, 2015.

[11] Y. Liu and R. Weyers. Modeling the time-to-corrosion cracking in chloride contaminated reinforced concrete structures. *ACI Materials Journal*, 95(6):675–680, 1998.

[12] Karin Lundgren. Bond between ribbed bars and concrete. part 2: The effect of corrosion. *Magazine of Concrete Research*, 57(7):383–395, 2005.

[13] A. Michel, B. J. Pease, A. Peterová, M. R. Geiker, H. Stang, and A. E. A. Thybo. Penetration of corrosion products and corrosion-induced cracking in reinforced cementitious materials: Experimental investigations and numerical simulations. *Cement and Concrete Composites*, 2013.

[14] F. Molina, C. Alonso, and C. Andrade. Cover cracking as a function of rebar corrosion: Part II-numerical model. *Materials and Structures*, 26(9):532–548, 1993.

[15] A. Mullard and M. G. Stewart. Corrosion-induced cover cracking: new test data and predictive models. *ACI Structural Journal*, 108(1):71, 2011.

[16] J. Ožbolt, F. Oršanić, G. Balabanić, and M. Kušter. Modeling damage in concrete caused by corrosion of reinforcement: Coupled 3D FE model. *International Journal of Fracture*, 178(1-2):233–244, 2012.

[17] S. J. Pantazopoulou and K. D. Papoulia. Modeling cover-cracking due to reinforcement corrosion in RC structures. *Journal of Engineering Mechanics*, 127(4):342–351, 2001.

[18] B. Šavija, M. Luković, J. Pacheco, and E. Schlangen. Cracking of the concrete cover due to reinforcement corrosion: a two-dimensional lattice model study. *Construction and Building Materials*, 44:626–638, 2013.

[19] E. Schlangen and J. G. M. van Mier. Simple lattice model for numerical simulation of fracture of concrete materials and structures. *Materials and Structures*, 25:534–542, 1992.

[20] K. Tran, H. Nakamura, K. Kawamura, and M. Kunieda. Analysis of crack propagation due to rebar corrosion using RBSM. *Cement and Concrete Composites*, 33(9):906–917, 2011.

[21] K. Tuutti. Corrosion of steel in concrete. Doctoral thesis, Swedish Cement and Concrete Research Institute, 1982.

[22] A. C. Ugural and S. K. Fenster. *Advanced Strength and Applied Elasticity. The SI Version*. Edward Arnold, 1981.

[23] P. A. Witherspoon, J. S. Y. Wang, K. Iawai, and J. E. Gale. Validity of cubic law for fluid flow in a deformable rock fracture. *Water Resour. Res*, 16(6):1016–1024, 1980.

[24] H. S. Wong, Y. X. Zhao, A. R. Karimi, N. R. Buenfeld, and W. L. Jin. On the penetration of corrosion products from reinforcing steel into concrete due to chloride-induced corrosion. *Corrosion Science*, 52:2469–2480, 2010.